Medical Engineering and Physics 73 (2019) 51–63

Contents lists available at ScienceDirect

Medical Engineering and Physics

journal homepage: www.elsevier.com/locate/medengphy

Significance of spine stability criteria on trunk muscle forces following unilateral muscle weakening: A comparison between kinematics-driven and stability-based kinematics-driven musculoskeletal models

Zeinab Kamal, Gholamreza Rouhi*

Faculty of Biomedical Engineering, Amirkabir University of Technology, Tehran, 11155-9567, Iran

ARTICLE INFO

Article history:
Received 27 October 2018
Revised 25 June 2019
Accepted 17 July 2019

Keywords:
Musculoskeletal model
Trunk stability
Kinematics
Optimization
Muscle weakness
Finite element model

ABSTRACT

Two optimization-driven approaches were employed to develop kinematics-driven (KD) and stability-based kinematics-driven (SKD) musculoskeletal models of an adult thoracolumbar to ascertain the significance of spine stability in holding the upright-standing posture after muscular disuse atrophy. Both models were used to estimate muscle forces of the trunk with intact and unilaterally reduced longissimus thoracis pars thoracic (LGPT) and multifidus lumborum (MFL) muscles strength. A finite element model of the L5–S1 segment of the same kinematics was also developed to compare the joint stresses predicted by the KD and SKD models. Matching well with *in vivo* data, the SKD model predicted a 15% and 33% reduction in contralateral muscle forces to the 95% debilitated LGPT and MFL muscles, respectively. In contrast, the contralateral muscle force enhancement to the debilitated MFL muscle in the KD model was in contradiction with *in vivo* data, implying that the KD model is incapable of correctly predicting the muscular disorders. However, the similarity of both models' predictions of intradiscal pressures and intervertebral discs' stresses, which matched well with *in vivo* data, does indicate the feasibility of the KD model to investigate trunk muscle weakness effects on spinal loads, which could offer additional tools for research in ergonomics. Nonetheless, SKD models can be employed for assessment of contralateral muscle impotence in spinal neuromuscular disorders.

1. Introduction

Weakening muscles by temporary muscular denervation is a common therapeutic approach to improve unilateral spinal spasticity, the most prevalently reported symptom for neuromuscular disorders of low-back paraspinal muscles [1,2]. Despite the breakthrough advantages of functional immobilization of the focal neurological lesion in spasticity disorders [3], some studies have reported that it might induce structural and mechanical muscle alterations [4] which can linger over time [3]. In addition, temporary muscular disuse atrophy in the spine may disrupt the balance of spinal loads generated by recruited muscles and result in segmental loss of stability [5,6]. Experiments on unilaterally focal Botulinum Toxin type A (BTX-A) injected rabbits have shown changes in muscle mass, strength, and structure of the target muscle as well as its contralateral hind limb [7]. The invasive, costly, and restricted nature of *in vivo* and *in vitro* measurements [8,9] has led to the emergence of musculoskeletal (MS) and passive (devoid of muscles) finite element (FE) models which can be used as viable complementary tools for noninvasive estimation of spinal loads and muscle forces [10]. Huynh et al. simulated the unilateral trunk muscle weakness in Duchenne muscular dystrophy using a combined MS and FE model of the spine and found an increase in abdominal muscles activation due to the unilaterally weakening of the erector spinae muscles [11]. While a number of biomechanical models have been employed to replicate the load carrying capacity of the spine [12], the effect of muscle weakness on a combined

Abbreviations: BTX-A, Botulinum Toxin type A; IDP, Intradiscal pressure; MS, Musculoskeletal; FE, Finite element; CT, Computed tomography; EOS, Electro optical system; IVD, Intervertebral disc; AF, Annulus fibrosis; NP, Nucleus pulposus; PCSA, Physiological cross-sectional area; KD, Kinematics-driven; SKD, Stability-based kinematics-driven; CAD, Computer-aided drawing; ICPT, Iliocostalis lumborum pars thoracic; LGPT, Longissimus thoracis pars thoracic; ICPL, Iliocostalis lumborum pars lumborum; LGPL, Longissimus thoracis pars lumborum; MFL, Multifidus lumborum; MFT, Multifidus thoracis; QL, Quadratus lumborum; IP, Iliopsoas; RA, Rectus abdominus; IO, Internal oblique; EO, External oblique.

* Corresponding author.
E-mail address: grouhi@aut.ac.ir (G. Rouhi).

https://doi.org/10.1016/j.medengphy.2019.07.008
1350-4533/

MS–FE model of the upright spine from a stability point of view has been nearly disregarded.

Segmental instability due to temporary functional immobilization of the spastic lesion most commonly occurs in the upper-extremity flexor muscles [2]. The longissimus thoracis pars thoracic (LGPT) muscle has been introduced as the most effective paraspinal muscle on spine stability in an upright-standing posture [13], which might be due to the bulk of stiffness provided by large muscles [6]. Furthermore, the activity of small intrinsic muscles is also necessary to maintain spine stability [6]. Among deep fibers, the multifidus (MFL) muscle acts as a primary stabilizing muscle in the spine [14]. In an experimental effort by Ward et al. on the lumbar spines of eight cadavers, the MFL muscle function was found to be crucial in the dynamic stabilization of the lumbar spine [15]. Therefore, weakened LGPT and MFL muscles can be considered critical candidates in the investigation of the importance of stability in a spine with unilaterally muscular disuse atrophy.

The purpose of this study was to estimate muscle forces in an adult thoracolumbar in an upright-standing position, and to compare the effects of unilateral LGPT and MFL muscle weakness on trunk muscle forces using a non-linear, 3D, six-joint kinematics-driven (KD) model and a stability-based kinematics-driven (SKD) MS model of an adult spine. Both models were also combined with an FE model of the L5–S1 segment of the same kinematics. In this work, it was hypothesized that introducing stability requirements into the optimization algorithm, *i.e.*, an SKD model *vs* a KD model, would provide a more realistic prediction of spinal muscle forces, in the case of unilateral muscle weakening. To the best of our knowledge, the effects of muscular disuse atrophy on spinal muscle forces have not been investigated in a stability-based MS model to date. Two analyses were used to investigate the validity of the hypothesis made in this study:

1. Muscle forces, L3–L4 and L4–L5 intradiscal pressures (IDPs), the relationship between loss of muscle strength and mass, and changes in muscle forces due to the target muscle weakening as well as the shear and compressive loads at T12–L1 thorough L5–S1 levels were investigated using KD and SKD musculoskeletal models and compared with *in vivo* data [7,16–21].
2. By applying equivalent loads, estimated by both KD and SKD musculoskeletal models, on the FE model of a spine, the von Mises stress and IDP at the L5–S1 level were investigated in models with intact and unilaterally weakened LGPT and MFL muscles in an upright-standing posture.

2. Method

2.1. Musculoskeletal model of the trunk

A sagittally-symmetric, non-linear 3D, six-joint (T12–L1 through L5–S1), musculoskeletal model was developed based on the geometry of a healthy male (52 years, 174.5 cm, and 68.4 kg) using MATLAB scripting (MATLAB® R2014b, Mathworks Inc., Natick, MA, US) to estimate muscle forces and eccentrically distributed gravity loading in a neutral upright posture [22], which is the least stable position of the spine [23]. The attachment sites of muscle fascicles to the bones were speculated based on parametric anatomical studies of a musculoskeletal spine [24–26] (Fig. 1). The entire thorax and total of bony structures were assumed to be rigid, and all six intervertebral discs were assumed to have non-linear rotational stiffness in three directions [22]. The physiological cross-sectional areas (PCSAs) of the muscles were extracted from the literature [27].

2.2. Optimization procedures constrained to equilibrium and stability requirements

Muscle forces in the upright-standing posture were estimated using an optimization algorithm constrained to equilibrium and stability conditions [22,28]. The moment equilibrium equations were written in three directions at each level for six joints, *i.e.*, T12–L1 through L5–S1 (Fig. 1). The joints' centroids were assumed as the geometric centers of the intervertebral discs (IVDs) [29]. Optimization formulations were used in Matlab (*fmincon* algorithm) to minimize summation of the cubed muscle stresses and to resolve the redundancy problem in the system of equations, which includes 92 unknown muscle forces but only 18 equilibrium equations, *i.e.*, 3 equilibrium equations at each level for six joints in the global *xyz* coordinate system (Fig. 1). Two optimization algorithms were written based on the kinematics-driven equilibrium and simultaneous consideration of KD and stability requirements (Equation (1)) to investigate the effects of unilateral muscle weakness on muscle forces. Equation (1) was used to optimize the muscle stresses in the MS model to meet equilibrium in the KD model and stability-based equilibrium in the SKD model of the spine [22]. The KD model was solved using Equation (1) without considering the stability criterion. Hence, muscle forces were estimated using the optimization algorithms while still satisfying physiological conditions on muscle forces.

$$min\left(\sum_{m=1}^{92}\left(\frac{F_m}{A_m}\right)^n\right)$$

$$subject\ to:\begin{cases}\sum M_i^{total}=0 & i=1,2,\ldots,18\\ F_{passive}\le F_m\le \sigma_{max}.A_m+F_{passive} & m=1,\ldots,92\\ eig(Hessian)>0 & Stability\ requirement\end{cases} \quad (1)$$

Equation (1) includes the unknown individual forces for each muscle (F_m); the muscle PCSA (A_m); the summation of all moments (M^{total}) at each joint about the IVD centroid in three directions; the passive force components ($F_{passive}$), assumed to be zero in the upright-standing position [22]; the maximum allowable muscle stress (σ_{max}), considered to be 0.6 MPa [22]; and the eigenvalues of the Hessian matrix of the potential energy, eig (Hessian), used as a stability criterion in the SKD model. The potential energy in the Hessian matrix of energy was determined from the passive torsional stiffness of the spine in an upright posture, muscle stiffness, and muscle forces [22,29] (Eq. (1)). Except for the stability criterion, the rest of the conditions of Equation (1) were similar in the KD and SKD models. To assure the results of muscle forces obtained by the optimization procedures were the global minimum, muscle forces were estimated using a genetic algorithm in MATLAB Optimization Toolbox™ (*genetic* algorithm), and compared with the results of muscle forces obtained by the KD and SKD constrained optimization procedures. Moreover, to ensure that muscle stresses did not exceed their physiological limits [22], muscle fiber stresses were computed by dividing the force over the PCSA of each muscle. Furthermore, knowing that the eigenvalues should be positive in order to be in a stable configuration [6], the eigenvalues of the Hessian matrix of the potential energy obtained by the KD model were also evaluated and analyzed.

In addition, as a means of replicating loading conditions *in vivo* the equivalent forces at the geometrical centers of T12–L1 through L5–S1 IVDs were approximated as a vector summation of muscle forces estimated by the MS models as well as the gravity loads at each level. The resultant equivalent loads were then divided over the disc areas at each level to estimate compressive and shear stresses on the T12–L1 through L5–S1 IVDs, as well as the intradiscal pressures at the L3–L4 through L5–S1 levels. In this

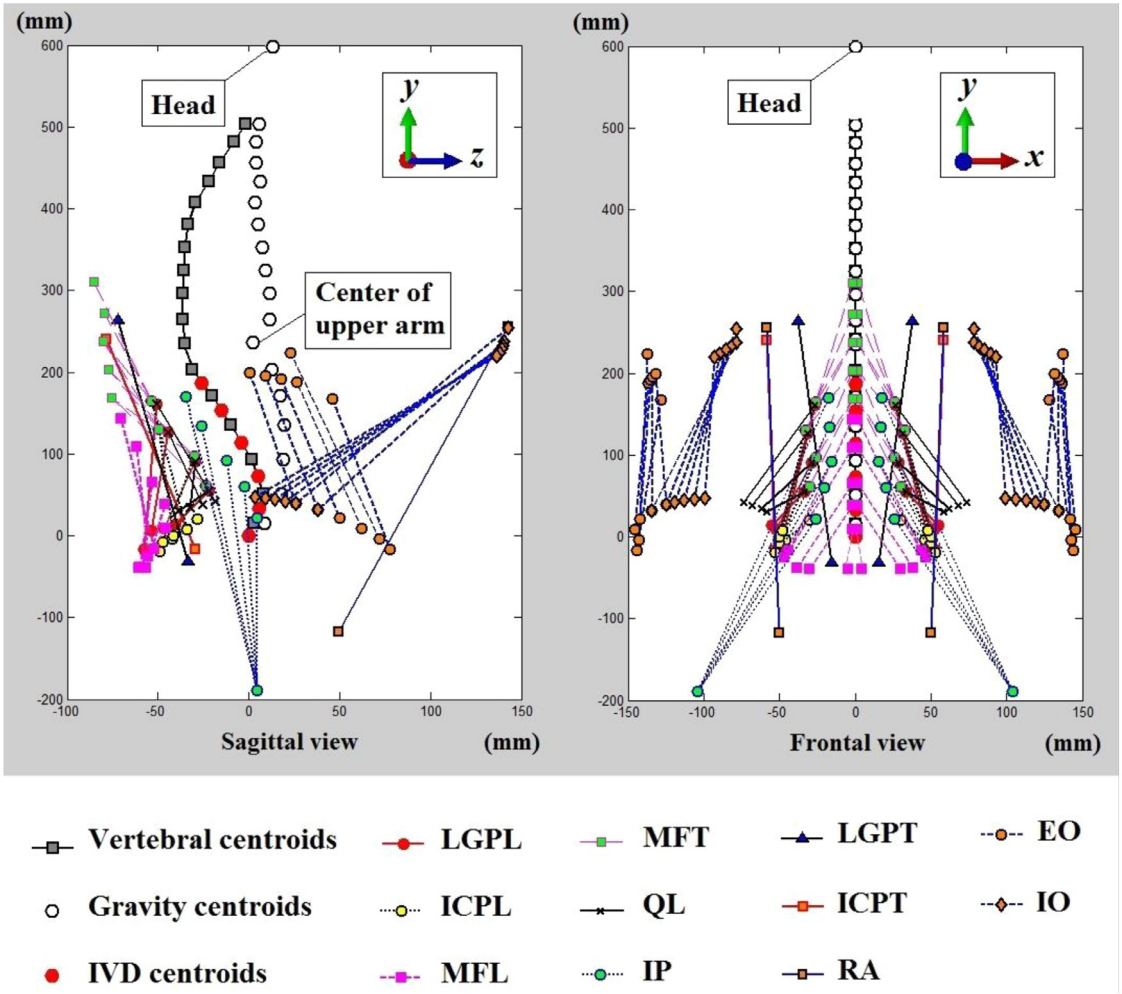

Fig. 1. The musculoskeletal (MS) model of the trunk in an upright-standing posture, in both sagittal and coronal views, with the center of gravity loads represented as white circular points in front of the vertebral column. The grey squares and red circles in the vertebral column are the position of vertebrae and intervertebral discs (IVDs), respectively, and were assumed as their geometric centroids [22]. Ninety-two bilateral distinct fascicles were used to simulate the muscles of the trunk. Sixty-two bilateral fascicles of local muscles were attached to the lumbar vertebrae (LGPL: longissimus thoracis pars lumborum; ICPL: iliocostalis lumborum pars lumborum; MFL: multifidus lumborum; MFT: multifidus thoracis; QL: quadratus lumborum; and IP: iliopsoas), and thirty bilateral fascicles of global muscles were connected to the thoracic spine and cage, including global back muscles (LGPT: longissimus thoracis pars thoracic and ICPT: iliocostalis lumborum pars thoracic), and global abdominal muscles (IO: internal oblique; EO: external oblique; and RA: rectus abdominus) [22]. The global *xyz* directions are shown in both sagittal and coronal views.

study, the compressive stresses predicted by the MS models, with a correction factor of 0.66 [27], were considered as the IDP at each level [22].

2.3. Weakening procedures of muscles

In order to be able to make a comparison between the outcomes of this study simulations and *in vivo* experimental data on the loss of strength in the BTX-A injected muscles of rabbits [7], the PCSAs of target LGPT and MFL muscles were gradually reduced by a reduction percentage of 0.5% to assign similar magnitudes of 88%, 89%, and 95% reduction in the target muscle forces to match the magnitudes of loss of strength in the rabbits [7]. The change in the muscle's PCSA was supposed to be proportional to the change in the muscle mass, assuming a constant muscle density and length.

2.4. Finite element model of L5–S1

A sagittally-symmetric passive FE model of the L5–S1 segment was developed to compare the effect of the KD and SKD musculoskeletal models' predictions on stress distribution within the basement joint, *i.e.*, the L5–S1 segment. The main reason for choosing the L5–S1 segment was that all muscle fascicles, and therefore all muscle forces, are present at this level (Fig. 1). The equivalent forces at the geometrical center of L5–S1 IVD, estimated by MS models, were then used in the FE model. The computer-aided drawing (CAD) parts of the basement vertebrae, *i.e.*, L5 and sacrum bones, were developed based on computed tomography (CT) images (0.6 mm slice thickness) of an adult thoracolumbar with the same kinematics in the supine posture using Mimics (Materialize, V10.01). Additionally, using Electro Optical System (EOS) imaging software (EOS imaging Co., France, Stereo Radiographic Patient Imaging), EOS images of the same trunk were used to re-align the CAD parts of the vertebrae to have similar inclinations in the anatomical planes to the upright-standing position (Fig. 2). In order to assure that the selected lumbar spine was in a balanced state, values of the sagittal alignment parameters of the curvature, *i.e.*, lumbar lordosis, sacral slope, and pelvic incidence (Fig. 2(a)), were checked and found to be in the normal ranges for each parameter as reported in the literature [30–33]. The institutional Ethics Committee approval and informed consent of the subject were obtained. Subsequently, the L5–S1 IVD, consisting of an annulus fibrosis (AF) and a nucleus pulposus (NP), were developed in Catia

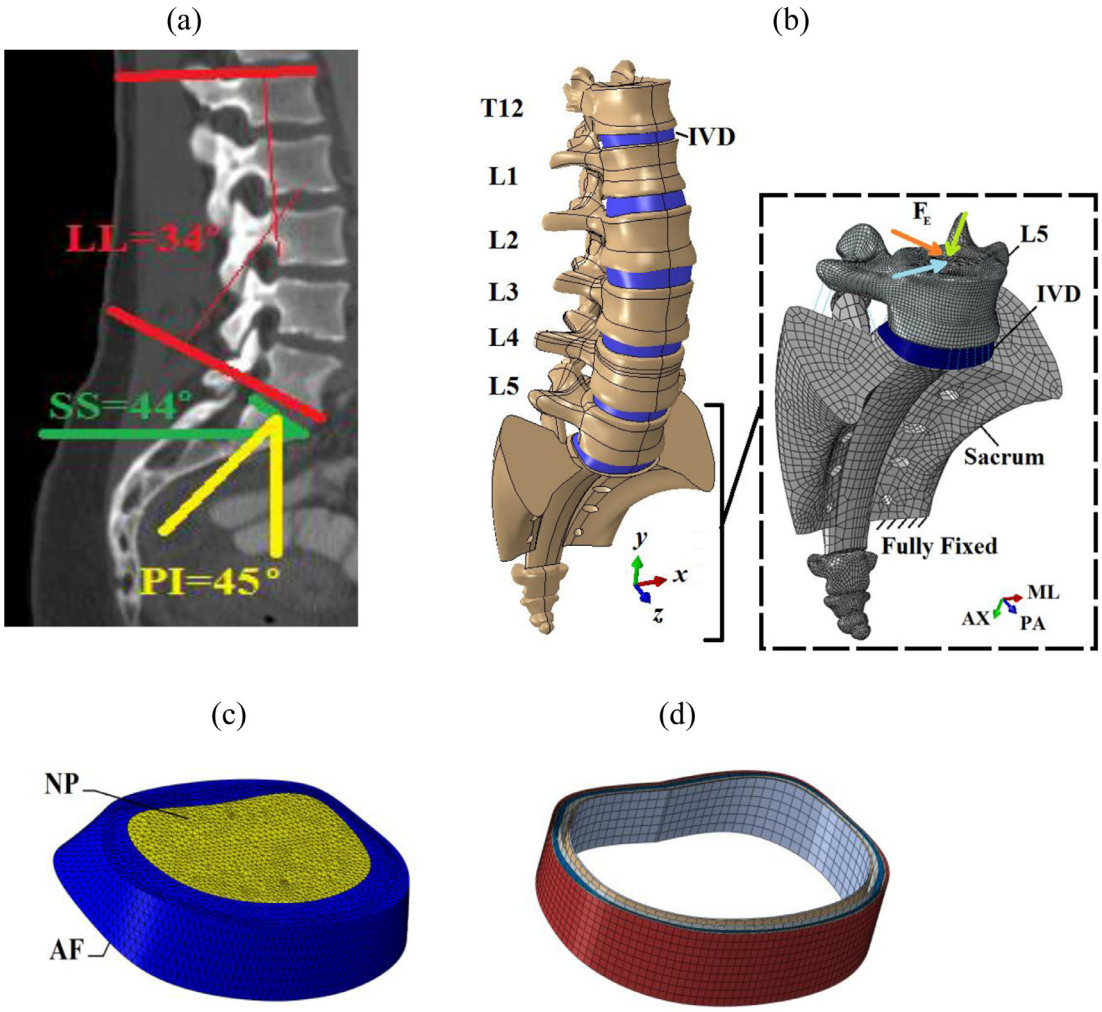

Fig. 2. (a) CT image of a normal spine in the sagittal plane, in which LL, SS, and PI represent the lumbar lordosis, sacral slope, and pelvic incidence, respectively. (b) Model of the lumbosacral spine in the global *xyz* coordinate system showing the FE model of the L5–S1 motion segment with the concentrated equivalent forces (FE) on the upper surface of L5 in local directions. ML, AX, and PA stand for local mediolateral, axial, and posteroanterior directions at each level, respectively. (c) FE models of the annulus fibrosis (AF) and nucleus pulposus (NP) of the L5–S1 intervertebral disc (IVD), and (d) the rebar embedded by membrane elements.

(Dassault Systèmes®, Vélizy-Villacoublay, France, V5R20) (Fig. 2). To analyze the model, the CAD parts of the bones and IVD were imported into computer-aided engineering software (ABAQUS 6.10, ABAQUS Inc., Providence, RI, USA). All bony structures were assumed to be rigid [22], with an element type of R3D4. The material of the IVD was assumed to be hyperelastic (Mooney–Rivlin), with a C10 and C01 of 0.18 MPa and 0.045 MPa, respectively, for AF [34] with an element type of C3D10, and 0.12 MPa and 0.030 MPa, respectively, for NP [35] with an element type of C3D10H. The annular fibers were simulated with rebar elements (modulus of elasticity and Poisson's ratio of 500 MPa and 0.45, respectively, with a crosswise pattern at ±30°) [36], which were distributed in the concentric lamellae embedded with membrane elements in AF [37] (Fig. 2). Sensitivity analysis was performed by increasing the number of elements to make sure that mesh size had no effect on the model outputs which resulted in 1840 and 2160 elements for AF and NP, respectively. The ligaments were modeled as sets of wires by axial nonlinear tension-only connector elements [38]. The ligaments included in the models were the anterior longitudinal, posterior longitudinal, capsular, flaval, and interspinous [37] (Fig. 2(b)). The sacrum was considered fully-constrained in the static analyses (Fig. 2(b)). Muscle forces, found by the MS models, and the gravity load at the L5–S1 level, used by scaling the magnitudes of the *in vivo* measurements [24], were prescribed into the subject-specific FE model as concentrated forces (Fig. 2(b)) to estimate stress distribution within L5–S1 IVD.

3. Results

3.1. Muscle forces of the KD and SKD models

Forces of abdominal and back muscles, introduced in Figure 1, determined by the KD and SKD models can be found in Figure 3. Also seen in Figure 3, and dissimilar to the KD model, the introduction of the stability criterion in the optimization algorithm results in abdominal muscles activation in the SKD model.

3.1.1. Target and contralateral muscle forces of the weakened models

Results of the SKD model showed loss of strength in the contralateral muscles to both target weakened LGPT and MFL muscles; but in contrast, the contralateral MFL muscle force increased by weakening the target muscle in the KD model (Fig. 4). Figure 4 shows the changes on each bar calculated using Equation (2), where F_{intact} and $F_{weakened}$ represent the forces of muscles on each side of the spine with intact and weakened muscles, respectively:

$$Change\ (\%) = \frac{F_{weakened} - F_{intact}}{F_{intact}}\ (\%) \qquad (2)$$

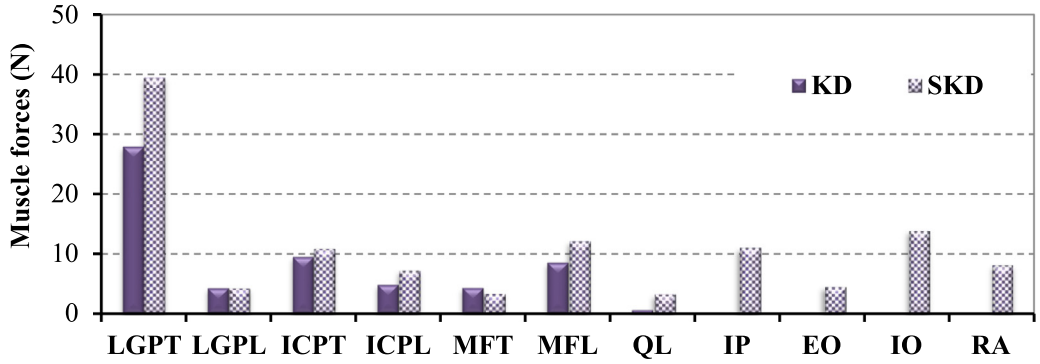

Fig. 3. Muscle forces determined by the kinematics-driven (KD) and stability-based kinematics-driven (SKD) musculoskeletal models.

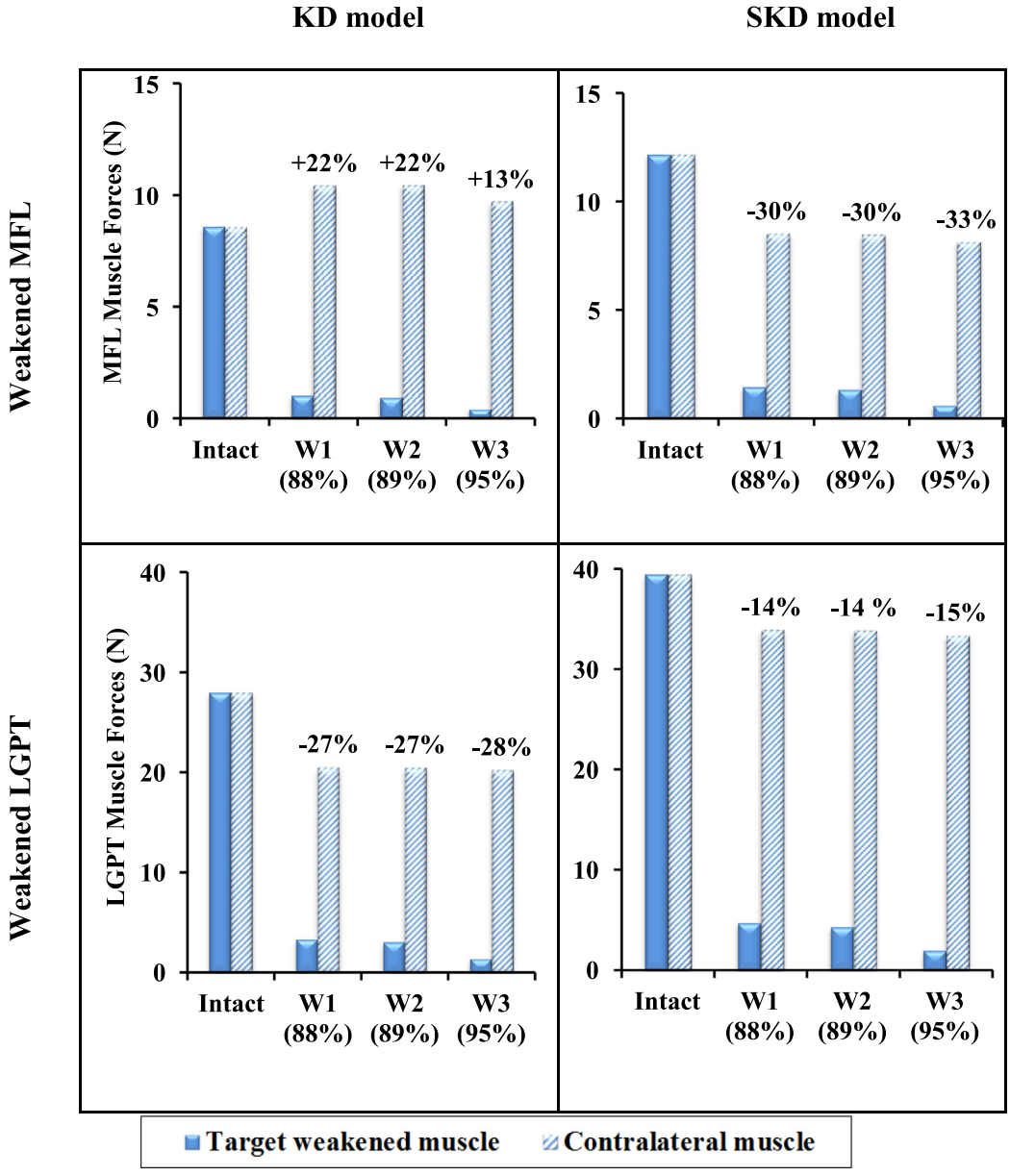

Fig. 4. Forces of the target and contralateral MFL (Top) and LGPT (Bottom) muscles of the: (Left) kinematics-driven (KD) and (Right) stability-based kinematics-driven (SKD) musculoskeletal models for intact and three target muscle weakening procedures with their percentage of change (see Eq. (2)) in the contralateral muscle forces on each bar. W1, W2, and W3 represent the weakened musculoskeletal models with an 88%, 89%, and 95% reduction in the target LGPT and MFL muscles forces, respectively.

3.1.2. Muscular contributions

In order to investigate the effects of unilateral muscle weakness on the force of the rest of the individual muscles, based on the experimental data of the loss of strength in rabbits' BTX-A injected muscles [7], the case of 95% reduction in MFL and LGPT muscle forces was investigated and the results of the simulation can be seen in Figure 5.

Percentage of change, defined by Equation (2), in the force of each muscle at the basement, *i.e.*, the L5–S1 level, where all muscle fascicles are present, due to a 95% reduction in the target muscle force in the KD and SKD musculoskeletal models can be found in Figure 6.

The maximum stress in the muscle fibers, with intact muscles, predicted by the KD and SKD musculoskeletal models were 0.08 and 0.10 MPa, respectively. After unilaterally muscle weakening, the maximum muscle fiber stress in the KD and SKD musculoskeletal models changed to 0.05 and 0.06 MPa, respectively, in the models with a weakened MFL muscle, and 0.06 and 0.07 MPa in the models with a weakened LGPT muscle.

With regard to the eigenvalues associated with the Hessian matrix for the KD and SKD musculoskeletal models, it was found that, in both cases of intact and weakened muscles, the smallest eigenvalues of the Hessian matrices associated with the KD model were all negative as opposed to those of the SKD model which were all positive due to the constraint considered in the optimization process.

3.2. Equivalent loads and IDPs in the MS and FE models

The equivalent forces at the geometrical centers of T12–L1 through L5–S1 IVDs were determined as a vector summation of the gravity loads along with the muscle forces, estimated by MS models, at each level (Fig. 7).

By finding the resultant equivalent forces caused by the vector summation of gravity and muscle forces over the disc area at each level, the compressive and shear stresses on T12–L1 through L5–S1 IVDs predicted by KD and SKD musculoskeletal models with intact muscles (Fig. 7) were compared to another study [39] on normal subjects (Fig. 8). The compressive stresses at the L3–L4 and L4–L5 levels, predicted by the MS models and with a correction factor of 0.66 [27], were considered as the IDPs and compared with *in vivo* data from the same levels of an upright spine [16–21] (Fig. 8). The IDPs at the L3–L4 and L4–L5 levels of the SKD models were found to be 27.1% and 24.2% greater than those of the KD models, respectively. Moreover, the IDPs at the L3–L4 and L4–L5 levels were found to be similar in the models with intact and weakened muscles.

By applying the equivalent forces, estimated by KD and SKD musculoskeletal models (Fig. 7), on the FE model of the L5–S1 IVD, the maximum stresses were found to appear in the outermost posterior layers of the annulus fibrosis for all six models of the spine (Fig. 9).

The stress distribution and IDPs in the FE model of the L5–S1 segment were found to be similar in both models with intact and weakened muscles (Fig. 9). The IDP at the L5–S1 level of the SKD model predicted by the FE (Fig. 9) and MS (Fig. 8) models was found to be 20.9% and 21.2% greater than those of the KD model, respectively.

3.3. Loss of target muscle mass and strength

The correlation between reduction in mass and strength of the target weakened muscles of both KD and SKD musculoskeletal models compared with the experimental data on BTX-A injected lower extremities of rabbits [7] can be seen in Figure 10.

4. Discussion

The effect of temporary muscle weakening, as a common treatment to improve unilateral spinal spasticity in neuromuscular disorders [1,2], has not been numerically investigated on upright spine stability to date. The aim of this study was to evaluate muscle forces in a spine with intact and unilaterally debilitated muscles using a kinematics-driven and stability-based kinematics-driven musculoskeletal model of a healthy adult male spine. It was hypothesized that employing stability requirements in the optimization algorithm, *i.e.*, an SKD model *vs* a KD model, would provide an indispensable tool to deliver a more realistic prediction of the unilateral muscle weakness effects on overall spinal muscle forces. To test the hypothesis, longissimus thoracis pars thoracic and multifidus lumborum muscles, as the muscles with the greatest impact on spine stability [13–15], were selected to be unilaterally weakened. KD and SKD musculoskeletal models were then used to estimate the muscle forces of the trunk with intact and unilaterally debilitated LGPT and MFL muscle strength. The equivalent forces at the geometrical centers of T12–L1 through L5–S1 intervertebral discs were approximated as a vector summation of muscle forces estimated by musculoskeletal models along with gravity loads at each level. The resultant equivalent loads (as an alternative to *in vivo* loads) were then divided over the disc areas at each level to estimate the compressive and shear stresses on T12–L1 through L5–S1 IVDs. In this study, the compressive stresses predicted by the MS models, with a correction factor of 0.66 [27], were considered as the intradiscal pressures at these levels [22]. In order to compare the effect of the KD and SKD model predictions on the stress distribution within the L5–S1 IVD where all muscle fascicles are present, a passive subject-specific FE model of the L5–S1 segment was developed and analyzed under the equivalent loads at the same level. The more compatible results of the stability-based model, regarding the contralateral muscle impotence to the weakened muscles, matched the *in vivo* data [7] better than those of the KD model (Figs. 3 and 4). This reaffirms the validity of the study hypothesis which highlighted the necessity of including stability requirements in spine equilibrium equalities when investigating neuromuscular disorders. Moreover, the approximate similarity of the equivalent forces (Fig. 7) as well as the stress distribution on T12–L1 through L5–S1 IVDs (Figs. 8 and 9), as determined by both KD and SKD models, indicate the KD model's capability to investigate the effect of trunk muscle weakness on spinal loads.

4.1. Muscular contributions in the musculoskeletal models

In comparison to the SKD model, the KD model of the spine assigned less force to the back muscles assuming only equilibrium requirements in the optimization algorithm and ignoring abdominal muscles activation. This shows that it provides insufficient stiffness to remain in a stable configuration (Fig. 3). Furthermore, the KD model predicted an increase in the contralateral MFL muscle force to the target weakened muscle to retain a spine with unilaterally weakened muscles in its equilibrium position (Fig. 4), which is inconsistent with the *in vivo* data [7]. In contrast, results of the SKD model showed a loss of strength in the contralateral muscles to both weakened LGPT and MFL muscles (Fig. 4), which is in agreement with the *in vivo* experimental data on unilaterally BTX-A injected rabbits [7]. The reason for the contradiction between the KD and SKD models lies in the distinct roles of the abdominal muscles and the consequent adjustment of their activation in the SKD model due to the inclusion of the spinal stability requirement. More precisely, introducing a stability criterion into the optimization algorithm resulted in a counterbalancing of the abdominal and back muscles activation in a spine with unilaterally weakened

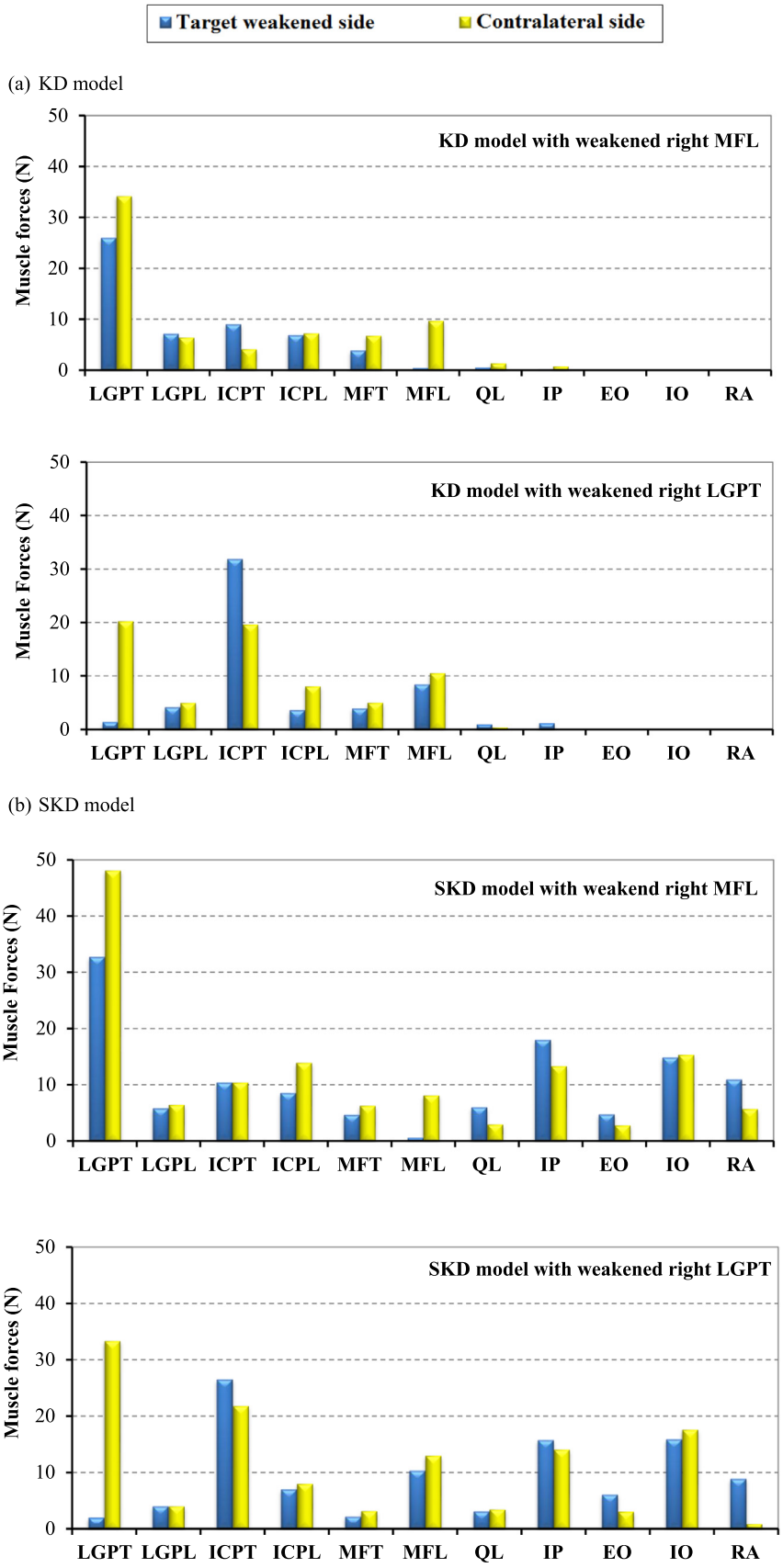

Fig. 5. Muscle forces of: (a) KD and (b) SKD musculoskeletal models assuming a 95% reduction in the force of the right MFL (Top a and b) and the right LGPT (Bottom a and b) muscles. The complete names of the muscles appear in Figure 1.

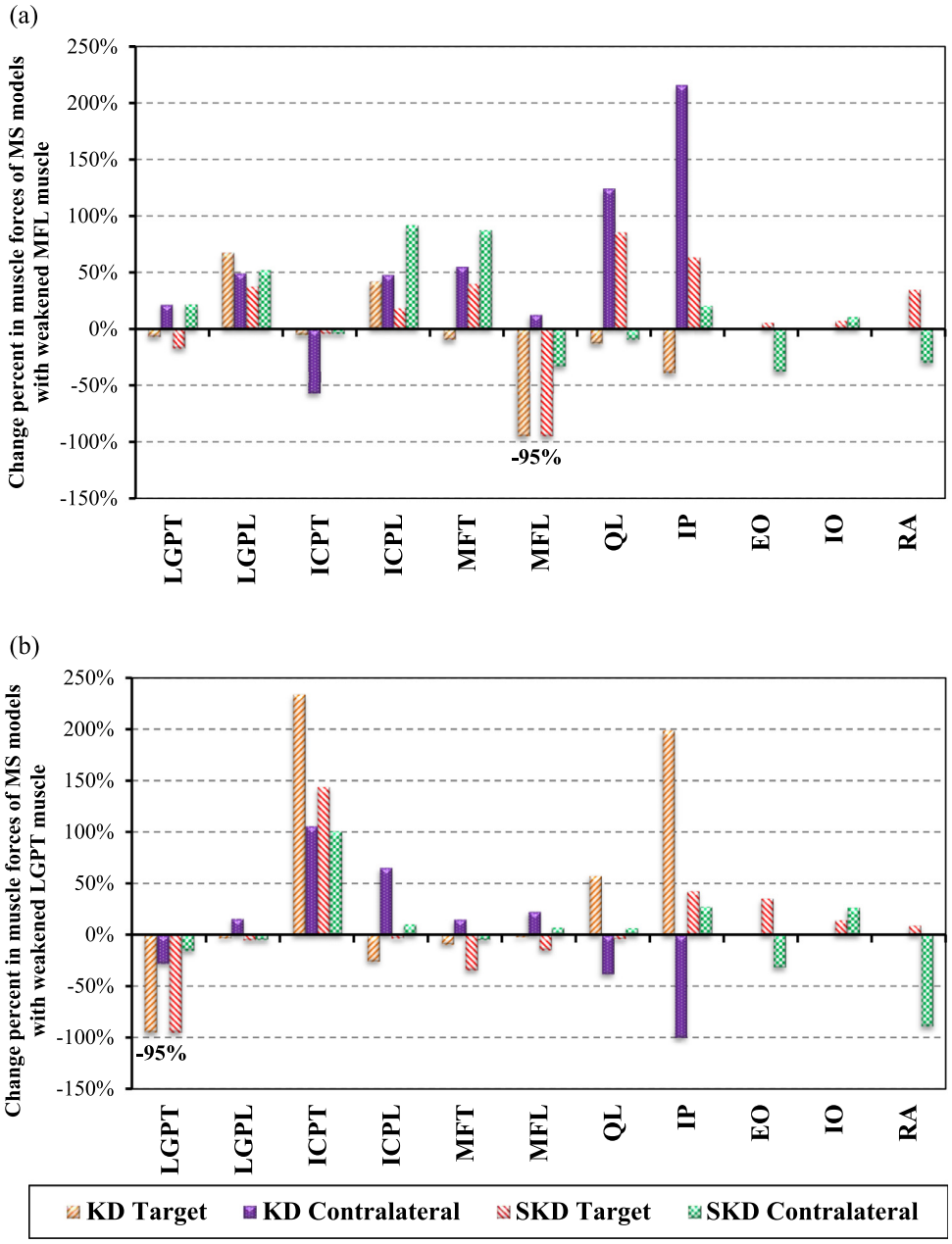

Fig. 6. Percentage of change in the force of each muscle (see Eq. (2)) due to a 95% reduction in the target MFL (Top) and LGPT (Bottom) muscle forces at the L5–S1 level of the KD and SKD musculoskeletal models. The complete names of the muscles appear in Figure 1.

muscles, which makes the SKD model capable of anticipating more realistic behavior of spinal muscles after unilateral muscle weakening. On the other hand, contralateral muscle force enhancement, predicted by the KD model, resembled the behavior of the contralateral muscles to strengthened muscles [40], and implied that the KD model was incapability of delineating the relevant assessment of contralateral muscle impotence in spinal neuromuscular disorders.

As can be seen in Figures 5 and 6, weakening of MFL and LGPT muscles in the SKD model caused smart changes in the overall force of the abdominal muscles to counterbalance the moments caused by the different contribution of the back muscles, which highlights the importance of antagonistic (abdominal) muscles activation in the upright spine stable position. The greater changes that occurred in the back muscle forces of the KD model, in contrast to the SKD model (see Figs. 5 and 6), can be explained by taking spine stiffness into account, which in the absence of abdominal muscles activation was provided by assigning greater changes to the contralateral back muscle forces in the KD model. In contrast, counterbalancing back and abdominal muscles activation after unilateral muscle weakening resulted in a smaller reduction in the muscle forces in the SKD model than in the KD model, and the subsequent stability of the SKD model (see Figs. 5 and 6). Furthermore, the maximum muscle fiber stress predicted by the KD and SKD models with intact and unilaterally weakened muscles varied only between 0.05 and 0.10 MPa, which does not exceed the maximum allowable muscle stress of 0.2–1.0 MPa [22,41]. Eigenvalues of the Hessian matrix of the KD model's potential energy were also evaluated to show the importance of introducing a stability criterion into the optimization algorithm of a spine with unilateral muscle weakness. Irrespective of if the muscles were intact or weakened, the smallest eigenvalue of the system of the KD

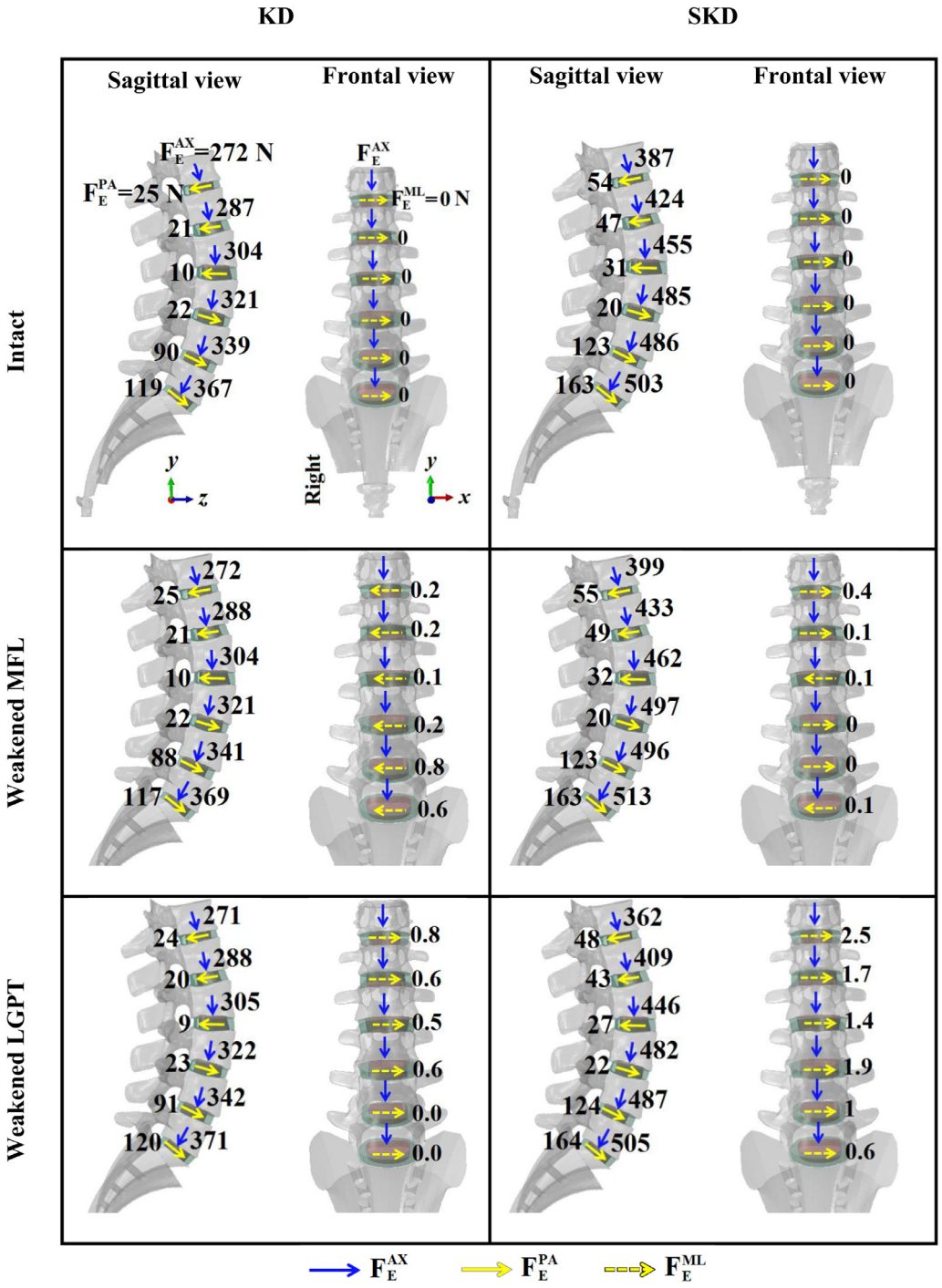

Fig. 7. The equivalent loads (F_E), consisting of the compressive load (F_E^{AX}) and shear loads of F_E^{PA} and F_E^{ML}, alongside the local axial (AX), posteroanterior (PA) and mediolateral (ML) directions at each level, as predicted by the KD (Left) and SKD (Right) musculoskeletal models with the intact (Top), unilaterally 95% debilitated MFL muscle (Middle), and LGPT muscle (Bottom). Note that ML, AX, and PA directions appear in Figure 2. All forces are given in *N*.

model was negative, which shows that the KD model's predictions do not meet the spine stability requirement. On the other hand, as expected due to the requirement imposed on Equation (1), *i.e.*, eig(Hessian) > 0, all eigenvalues of the SKD model were positive, which indicates that the unilateral muscle weakening did not disrupt spine stability. Accordingly, one can conclude that the KD model, as opposed to the SKD model, does not have the capability to anticipate realistic behavior of spinal muscles, for instance after unilateral muscle weakening, due to the lack of a stability requirement.

4.2. Effect of unilateral muscle weakening on the equivalent loads and IDPs

In order to indirectly check the validity of the combined MS–FE models, the equivalent shear and compressive loads were estimated at the geometrical centers of T12–L1 through L5–S1 IVDs (Fig. 7) and applied on each level as an alternative to the muscle force components and gravity loads to evaluate the IDPs (Fig. 9). The resultant shear and compressive loads at T12–L1 through L5–S1 levels (Fig. 7) were found to be in the physiological ranges of

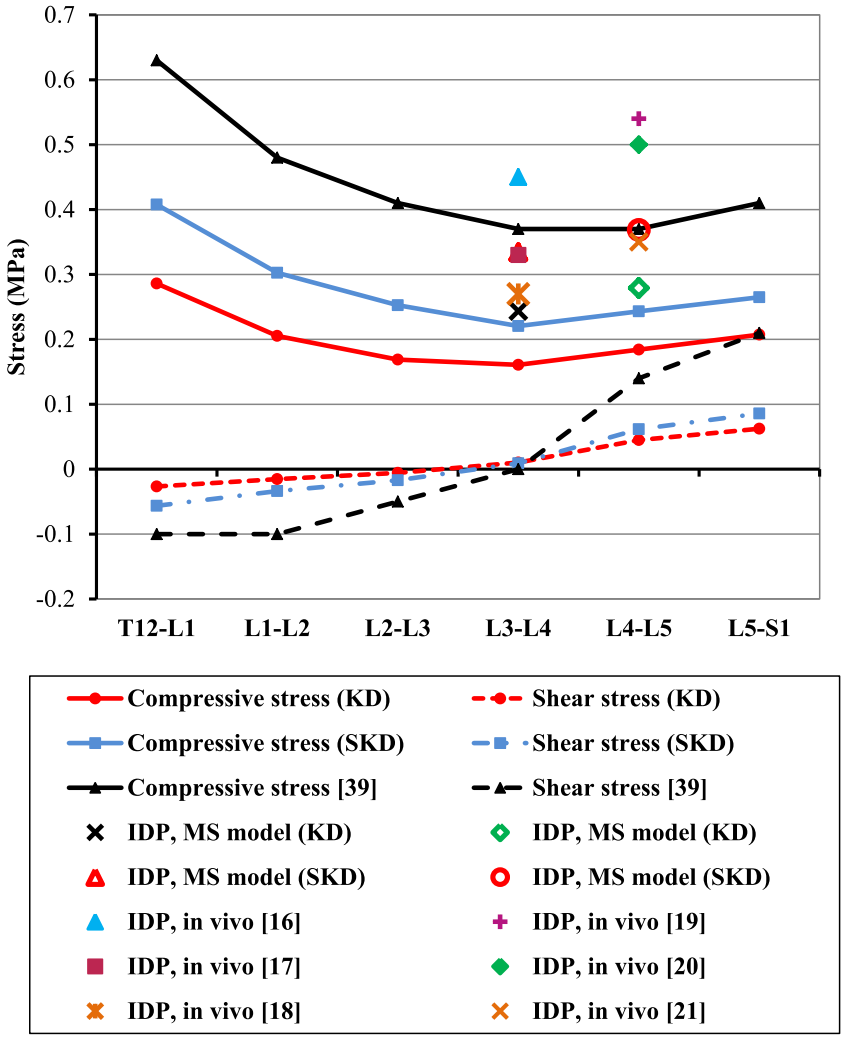

Fig. 8. The compressive (F_E^{AX}) and shear (F_E^{PA}) stresses on the lumbosacral IVDs as well as the IDPs at the L3–L4 and L4–L5 level of the intact musculoskeletal models alongside the local axial and posteroanterior directions at each level are compared to the literature [16–21,39].

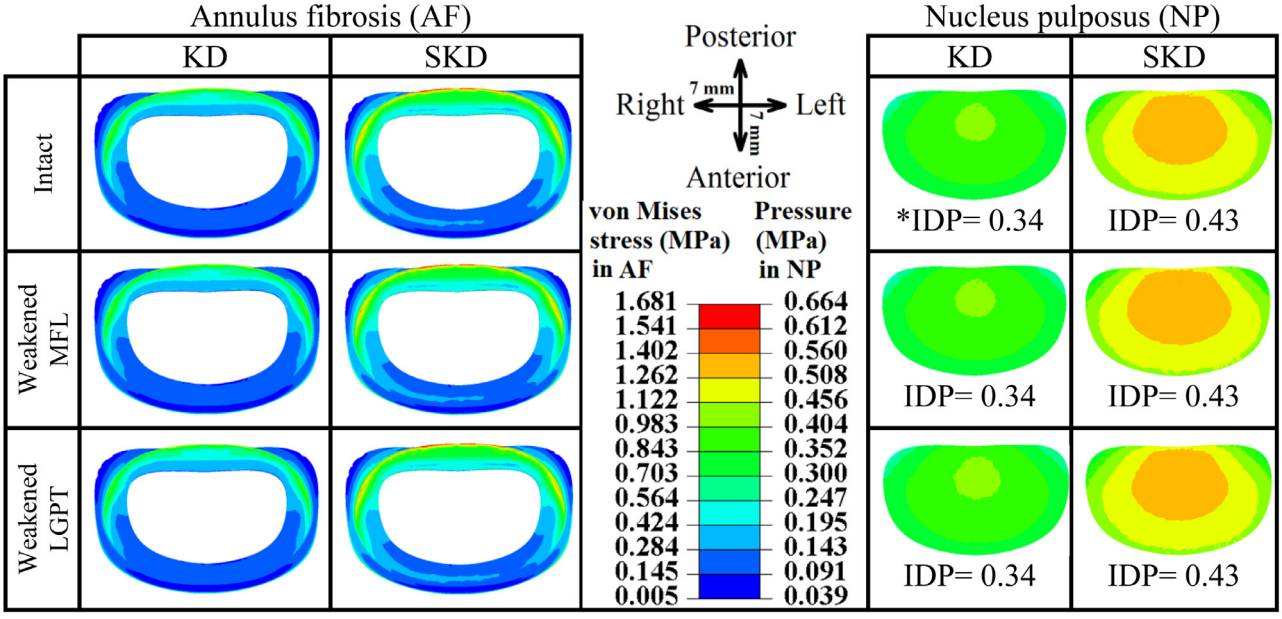

Fig. 9. Contour plots of von Mises stress and pressure in the annulus fibrosis (AF) and nucleus pulposus (NP) predicted by the FE model of the L5–S1 intervertebral disc under gravity load along with forces of intact muscles (Top), muscles with unilaterally debilitated MFL (Middle), and LGPT (Bottom) muscles as determined by the KD and SKD musculoskeletal models. *The intradiscal pressures (IDPs) are the average values of pressures in NPs.

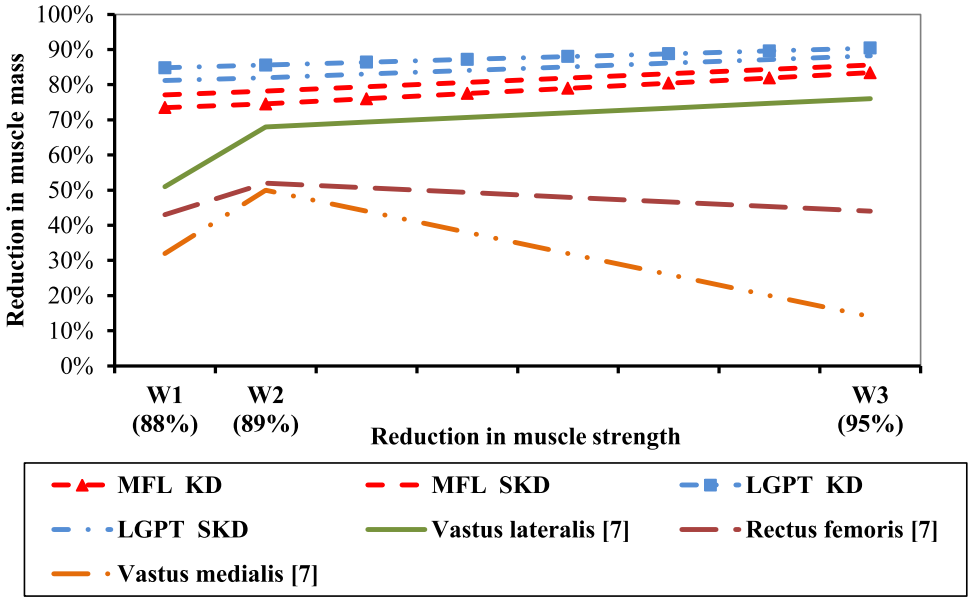

Fig. 10. Correlation between the loss of muscle mass and strength of the target weakened LGPT and MFL muscles of the KD and SKD musculoskeletal models compared to results obtained by experiments as reported by Fortuna et al. [7].

ultimate shear [42] and compressive strength [43], respectively. The compressive stresses, with a correction factor of 0.66 [27] and which were considered as IDPs [22,27], at the L3–L4 and L4–L5 levels were found by MS models to be ~0.24 and 0.28 MPa, respectively, in the KD model and 0.33 and 0.37 MPa, respectively, in the SKD model. These were similar for models with both intact and weakened muscles. Despite the similarity of equivalent forces in both MS models, the SKD model's IDPs at the L3–L4 and L4–L5 level agreed better with normal subject's *in vivo* data at the same levels than the KD model's IDPs at the L3–L4 and L4–L5 level (Fig. 8). This supports the necessity of introducing a stability criterion into the optimization algorithm.

The FE models of L5–S1 IVD predicted greater stresses under muscle forces estimated by SKD musculoskeletal models (Fig. 9) than muscles forces estimated by KD musculoskeletal models, this may be due to the greater equivalent loads in these models (Fig. 7). Furthermore, all six FE models of the spine predicted greater stress magnitude in the outermost posterior layers of the annulus fibrosis compared to other regions (Fig. 9), which agreed with results reported in the literature [39]. The SKD model's IDP at the L5–S1 level predicted by the FE and MS models was found to be 20.9% and 23.9%, respectively, greater than those of the KD model, which might be due to greater forces provided by back and abdominal muscles activation in the stability-based model (Figs. 3 and 5). In general, the approximate similarity of the equivalent loads (Fig. 7) and IDPs at the L3–L4 through L5–S1 levels (Figs. 8 and 9) as determined by both KD and SKD models implies that the KD model is capable of investigating the effects of trunk muscle weakness on spinal loads, which could provide an additional scope for biomechanical modeling applications in the ergonomics field [44].

4.3. Correlation between loss of target muscle mass and strength

Consistent with the early stages of muscle weakening in BTX-A injected rabbits [7], both KD and SKD models predicted a positive correlation between loss of strength and mass for both weakened LGPT and MFL muscles (Fig. 10). A similar loss of muscle mass and strength trend was found between the unilaterally weakened LGPT and MFL muscles in this study (Fig. 10) and the BTX-A injected rabbits' vastus lateralis muscle [7], which is the most effective quadriceps muscle in providing stability in the upright position [45]. In contradiction to this study's predictions, the descending trend of rectus femoris and vastus medialis muscles in the later stages of BTX-A injections might be due to the association between repeated BTX-A injections, muscle disuse atrophy, and loss of weakened muscle characteristics [7].

4.4. Limitations

Due to the paucity of *in vivo* data in the current literature, the results of this study were compared with the experimental data on unilaterally BTX-A injected rabbits' hind limbs [7] (Fig. 10), despite the limited capability of animal studies to predict chemical drug effects on humans [46] and the difference in the stable position of animal and human spines [47]. Results of the SKD model showed a fairly good agreement with the experimental data on animals [7] and humans [16–21], implying that introducing stability criterion into the optimization algorithm made it feasible for MS models to predict spinal loads (Fig. 8) and the contralateral muscle impotence to the weakened muscles (Figs. 4–6). The greater loss in the contralateral muscle strength of repeated BTX-A injected rabbits [7] than that found in the current study suggests that muscle disuse atrophy may deteriorate both weakened and contralateral muscles characteristics. In other words, aggravation of contralateral attributes, ignored in the current study, may lead to a number of physiological changes in skeletal muscle function [48], and thus a greater loss in the contralateral muscles forces. Another discrepancy between this work and a previous study [7] goes back to the ways these two studies looked at the problem, *i.e.*, a numerical investigation versus an experimental animal study [7]. In addition, due to the insignificant effect of ignoring the translational degrees of freedom on the accuracy of estimating spinal loads and stability in musculoskeletal models [49], only the rotational degrees of freedom were included in the analyses of this study. It should be noted that the human central nervous system strategy for changing muscle activity patterns to stabilize the spine beyond its critical buckling condition remains incompletely understood [50]. In order to overcome some of the shortcomings of this work, future theoretical and electromyographic studies should be made taking

into account the physiological effects of muscle disuse atrophy and loss of characteristics of both weakened and contralateral muscles in their human models.

5. Conclusion

In this study, the effects of unilateral weakening of the LGPT and MFL muscles on overall muscle forces were investigated in an adult thoracolumbar using a non-linear, 3D, six-joint kinematics-driven and a stability-based kinematics-driven MS model combined with a passive FE model of the spine. Both SKD and KD models could predict back muscle activities (Fig. 3) and IDPs (Fig. 9) in agreement with the literature [16–21]. Nonetheless, in contrast to the KD model, the SKD model provided a more realistic assessment for contralateral muscle impotence (Figs. 4 and 9) and IDPs (Fig. 8) implying that the SKD model has a stronger capability to investigate focal muscular disorders. However, the approximate similarity of predicted equivalent loads (Fig. 7) and lumbosacral discs' stresses (Figs. 8 and 9) by both models illustrated the feasibility of using the KD model to investigate the effect of trunk muscle weakness on spinal loads, which could provide a new scope for biomechanical modeling applications in the field of ergonomics [44]. Due to the limitations of non-invasive procedures to assess the effects of unilateral muscle weakening on spine biomechanics [51], it is hoped that the current stability-based kinematics-driven approach will be able to enhance our insight into the complex mechanisms behind muscles activation in the upright-standing posture as well as shed some light on the effects of muscular weakness on osteoarthritis.

Ethical approval

The study was approved by the ethics committee of Amirkabir University of Technology and written informed consent obtained from the subject on whose data the model is based.

Acknowledgment

This work was supported by the Amirkabir University of Technology. The authors would also like to appreciate Dr. Mohammad Parnianpour, Dr. Navid Arjmand, and Dr. Mohammadali Erfani for their constructive comments and support.

Conflict of interest

The authors have no conflicts of interest relevant to this article to report.

Supplementary material

Supplementary material associated with this article can be found, in the online version, at doi:10.1016/j.medengphy.2019.07.008.

References

[1] Jabbari B. Treatment of chronic low back pain with botulinum neurotoxins. Curr Pain Headache Rep 2007;11(5):352–8.
[2] Elbasiouny SM, Moroz D, Bakr MM, Mushahwar VK. Management of spasticity after spinal cord injury: current techniques and future directions. Neurorehabil Neural Repair 2010;24(1):23–33. doi:10.1177/1545968309343213.
[3] Colhado OCG, Boeing M, Ortega LB. Botulinum toxin in pain treatment. Rev Bras Anestesiol 2009;59(3):366–81. doi:10.1590/S0034-70942009000300013.
[4] Lieber RL, Steinman S, Barash IA, Chambers H. Structural and functional changes in spastic skeletal muscle. Muscle Nerve 2004;29(5):615–27. doi:10.1002/mus.20059.
[5] Moreland JD, Richardson JA, Goldsmith CH, Clase CM. Muscle weakness and falls in older adults: a systematic review and meta-analysis. J Am Geriatr Soc 2004;52(7):1121–9. doi:10.1111/j.1532-5415.2004.52310.x.
[6] Cholewicki J, McGill SM. Mechanical stability of the in vivo lumbar spine: implications for injury and chronic low back pain. Clin Biomech 1996;11:1–15. doi:10.1016/0268-0033(95)00035-6.
[7] Fortuna R, Vaz MA, Youssef AR, Longino D, Herzog W. Changes in contractile properties of muscles receiving repeat injections of botulinum toxin (Botox). J Biomech 2011;44:39–44. doi:10.1016/j.jbiomech.2010.08.020.
[8] Rohlmann A, Graichen F, Kayser R, Bender A, Bergmann G. Loads on a telemeterized vertebral body replacement measured in two patients. Spine 2008;33:1170–9. doi:10.1097/BRS.0b013e3181722d52.
[9] Wilke HJ, Rohlmann A, Neller S, Graichen F, Claes L, Bergmann G. ISSLS prize winner: a novel approach to determine trunk muscle forces during flexion and extension: a comparison of data from an in vitro experiment and in vivo measurements. Spine (Phila Pa 1976) 2003;28(23):2585–93. doi:10.1097/01.BRS.0000096673.16363.C7.
[10] Wang K, Jiang C, Wang L, Wang H, Niu W. The biomechanical influence of anterior vertebral body osteophytes on the lumbar spine: a finite element study. Spine J 2018;18(12):2288–96. doi:10.1016/j.spinee.2018.07.001.
[11] Huynh AM, Aubin CE, Mathieu PA, Labelle H. Simulation of progressive spinal deformities in Duchenne muscular dystrophy using a biomechanical model integrating muscles and vertebral growth modulation. Clin Biomech 2007;22(4):392–9. doi:10.1016/j.clinbiomech.2006.11.010.
[12] Dreischarf M, Shirazi-Adl A, Arjmand N, Rohlmann A, Schmidt H. Estimation of loads on human lumbar spine: a review of in vivo and computational model studies. J Biomech 2016;49(6):833–45. doi:10.1016/j.jbiomech.2015.12.038.
[13] Cholewicki J, VanVliet JJ 4th. Relative contribution of trunk muscles to the stability of the lumbar spine during isometric exertions. Clin Biomech (Bristol, Avon) 2002;17(2):99–105. doi:10.1016/S0268-0033(01)00118-8.
[14] Masi AT, Nair K, Evans T, Ghandour Y. Clinical, biomechanical, and physiological translational interpretations of human resting myofascial tone or tension. Int J Ther Massage Bodyw 2010;3(4):16–28.
[15] Ward SR, Kim CW, Eng CM, Gottschalk LJ 4th, Tomiya A, Garfin SR, Lieber RL. Architectural analysis and intraoperative measurements demonstrate the unique design of the multifidus muscle for lumbar spine stability. J Bone Joint Surg Am 2009;91(1):176–85. doi:10.2106/JBJS.G.01311.
[16] Nachemson A, Elfström G. Intravital dynamic pressure measurements in lumbar discs. A study of common movements, maneuvers and exercises. Scand J Rehabil Med Suppl 1970;1:1–40.
[17] Andersson GBJ, Örtengren R, Nachemson A. Quantitative studies of back loads in lifting. Spine 1976;1(3):137–88.
[18] Schultz A, Andersson G, Ortengren R, Haderspeck K, Nachemson A. Loads on the lumbar spine. Validation of a biomechanical analysis by measurements of intradiscal pressures and myoelectric signals. J Bone Joint Surg Am 1982;64(5):713–20.
[19] Sato K, Kikuchi S, Yonezawa T. In vivo intradiscal pressure measurement in healthy individuals and in patients with ongoing back problems. Spine (Phila Pa 1976) 1999;24(23):2468–74. doi:10.1097/00007632-199912010-00008.
[20] Wilke H, Neef P, Hinz B, Seidel H, Seidel H, Claes L. Intradiscal pressure together with anthropometric data-a data set for the validation of models. Clin Biomech (Bristol, Avon) 2001;16(Suppl 1):S111–26. doi:10.1016/S0268-0033(00)00103-0.
[21] Takahashi I, Kikuchi S, Sato K, Sato N. Mechanical load of the lumbar spine during forward bending motion of the trunk—a biomechanical study. Spine (Phila Pa 1976) 2006;31(1):18–23. doi:10.1097/01.brs.0000192636.69129.fb.
[22] Kamal Z, Rouhi G, Arjmand N, Adeeb S. A stability-based model of a growing spine with adolescent idiopathic scoliosis: a combined musculoskeletal and finite element approach. Med Eng Phys 2019;64:46–55. doi:10.1016/j.medengphy.2018.12.015.
[23] Schafer RC. Chapter 4: Body alignment, posture, and gait. In: Schafer RC, editor. Clinical biomechanics: musculoskeletal actions and reactions. Baltimore: Wiliams & Wilkins; 1987. p. 789.
[24] Bogduk N, Macintosh JE, Pearcy MJ. A universal model of the lumbar back muscles in the upright position. Spine (Phila Pa 1976) 1992;17(8):897–913.
[25] Chaffin DB, Redfern MS, Erig M, Goldstein SA. Lumbar muscle size and locations from CT scans of 96 women of age 40 to 63 years. Clin Biomech (Bristol, Avon) 1990;5(1):9–16. doi:10.1016/0268-0033(90)90026-3.
[26] Dumas GA, Poulin MJ, Roy B, Gagnon M, Jovanovic M. Orientation and moment arms of some trunk muscles. Spine (Phila Pa 1976) 1991;16(3):293–303. doi:10.1097/00007632-199103000-00007.
[27] Dreischarf M, Rohlmann A, Zhu R, Schmidt H, Zander T. Is it possible to estimate the compressive force in the lumbar spine from intradiscal pressure measurements? A finite element evaluation. Med Eng Phys 2013;35(9):1385–90. doi:10.1016/j.medengphy.2013.03.007.
[28] Zeinali-Davarani S, Hemami H, Barin K, Shirazi-Adl A, Parnianpour M. Dynamic stability of spine using stability-based optimization and muscle spindle reflex. IEEE Trans Neural Syst Rehabil Eng 2008;16(1):106–18. doi:10.1109/TNSRE.2007.906963.
[29] Stokes IAF, Gardner-Morse M. Lumbar spinal muscle activation synergies predicted by multi-criteria cost function. J Biomech 2001;34:733–40. doi:10.1016/S0021-9290(01)00034-3.
[30] Vrtovec T, Janssen MMA, Likar B, Castelein RM, Viergever MA, Pernuš F. A review of methods for evaluating the quantitative parameters of sagittal pelvic alignment. Spine J 2012;12(5):433–46. doi:10.1016/j.spinee.2012.02.013.
[31] Roussouly P, Berthonnaud E, Dimnet J. Geometrical and mechanical analysis of lumbar lordosis in an asymptomatic population: proposed classification. Rev Chir Orthop Reparatrice Appar Mot 2003;89(7):632–9.

[32] Roussouly P, Gollogly S, Berthonnaud E, Dimnet J. Classification of the normal variation in the sagittal alignment of the human lumbar spine and pelvis in the standing position. Spine (Phila Pa 1976) 2005;30(3):346–53. doi:10.1097/01.brs.0000152379.54463.65.
[33] Zhu R, Niu W, Wang Z, Pei X, He B, Zeng Z, Cheng L. The effect of muscle direction on the predictions of finite element model of human lumbar spine. Biomed Res Int 2018;2018:4517471. doi:10.1155/2018/4517471.
[34] El-Rich M, Arnoux P, Wagnac E, Brunet C, Aubin CE. Finite element investigation of the loading rate effect on the spinal load-sharing changes under impact conditions. J Biomech 2009;42(9):1252–62. doi:10.1016/j.jbiomech.2009.03.036.
[35] Schmidt H, Heuer F, Simon U, Kettler A, Rohlmann A, Claes L, Wilke HJ. Application of a new calibration method for a three-dimensional finite element model of a human lumbar annulus fibrosus. Clin Biomech (Bristol, Avon) 2006;21(4):337–44. doi:10.1016/j.clinbiomech.2005.12.001.
[36] Little JP, Adam CJ, Evans JH, Pettet GJ, Pearcy MJ. Nonlinear finite element analysis of anular lesions in the L4/5 intervertebral disc. J Biomech 2007;40(12):2744–51. doi:10.1016/j.jbiomech.2007.01.007.
[37] Kamal Z, Rouhi G. A parametric investigation on the effects of cervical disc prostheses with upward and downward nuclei on spine biomechanics. J Mech Med Biol 2015;16(2):1650092. doi:10.1142/S0219519416500925.
[38] Shirazi-Adl A, Ahmed AM, Shrivastava SC. Mechanical response of a lumbar motion segment in axial torque alone and combined with compression. Spine (Phila Pa 1976) 1986;11(9):914–27.
[39] Keller TS, Colloca CJ, Harrison DE, Janik TJ. Influence of spine morphology on intervertebral disc loads and stresses in asymptomatic adults: implications for the ideal spine. Spine J 2005;5(3):297–309. doi:10.1016/j.spinee.2004.10.050.
[40] Cirer-Sastre R, Beltrán-Garrido JV, Corbi F. Contralateral effects after unilateral strength training: a meta-analysis comparing training loads. J Sports Sci Med 2017;16(2):180–6.
[41] Zajak FE, Winters JM. Modeling musculoskeletal movement systems: joint and body segment dynamics, musculoskeletal actuation, and neuromuscular control. In: Winters JM, Woo SLY, editors. Multiple muscle systems: biomechanics and movement organization. New York: Springer-Verlag; 1990. p. 121–48.
[42] Gallagher S, Marras WS. Tolerance of the lumbar spine to shear: a review and recommended exposure limits. Clin Biomech (Bristol, Avon) 2012;27(10):973–8. doi:10.1016/j.clinbiomech.2012.08.009.
[43] Ayoub MM, Mital A. Manual materials handling. London: Taylor & Francis; 1989.
[44] Sachan A, Verma VK, Panda S, Singh K. Ergonomics, posture and exercises – pain free, prolong orthodontic career. J Orthod Res 2013;1(3):89–94. doi:10.4103/2321-3825.123318.
[45] Erskine RM, Jones DA, Maganaris CN, Degens H. In vivo specific tension of the human quadriceps muscle. Eur J Appl Physiol 2009;106(6):827–38. doi:10.1007/s00421-009-1085-7.
[46] Shanks N, Greek R, Greek J. Are animal models predictive for humans? Philo Ethics Humanit Med 2009;4:2. doi:10.1186/1747-5341-4-2.
[47] Sheng SR, Wang XY, Xu HZ, Zhu GQ, Zhou YF. Anatomy of large animal spines and its comparison to the human spine: a systematic review. Eur Spine J 2010;19(1):46–56. doi:10.1007/s00586-009-1192-5.
[48] Chang E, Ghosh N, Yanni D, Lee S, Alexandru D, Mozaffar T. A review of spasticity treatments: pharmacological and interventional approaches. Crit Rev Phys Rehabil Med 2013;25(1–2):11–22. doi:10.1615/CritRevPhysRehabilMed.2013007945.
[49] Ghezelbash F, Arjmand N, Shirazi-Adl A. Effect of intervertebral translational flexibilities on estimations of trunk muscle forces, kinematics, loads, and stability. Comput Methods Biomech Biomed Eng 2015;18(16):1760–7. doi:10.1080/10255842.2014.961440.
[50] Nordin AD, Rymer WZ, Biewener AA, Schwartz AB, Chen D, Horak FB. Biomechanics and neural control of movement, 20 years later: what have we learned and what has changed? J Neuroeng Rehabil 2017;14:91. doi:10.1186/s12984-017-0298-y.
[51] Fujita T, Sato A, Togashi Y, Kasahara R, Ohashi T, Yamamoto Y. Contribution of abdominal muscle strength to various activities of daily living of stroke patients with mild paralysis. J Phys Ther Sci 2015;27(3):815–18. doi:10.1589/jpts.27.815.